Effect of Initial Take-Up Speed on Properties and Structure of As-Spun and Drawn/Heat-Set Poly(ethylene terephthalate) Filaments

J. F. HOTTER,[1] J. A. CUCULO,[1] P. A. TUCKER,[1] B. K. ANNIS[2]

[1] North Carolina State University, College of Textiles, Raleigh, North Carolina 27695-8301

[2] Oak Ridge National Laboratory, Oak Ridge, Tennessee 37831-6197

Received 31 July 1997; accepted 30 December 1997

ABSTRACT: The effect of initial take-up speed on the properties and structure of both as-spun and drawn/heat-set poly(ethylene terephthalate) filaments was characterized through measurements of birefringence, percent crystallinity, tensile properties, high temperature shrinkage, loss tangent temperature dependence, DSC melting behavior, and wide-angle (WAXS) and small-angle X-ray scattering (SAXS). While a steady trend toward improved as-spun filament orientation and tensile properties occurred with increasing initial take-up speed, the reduced drawability of these more structured precursor filaments resulted in corresponding drawn/heat-set filaments that were of relatively lower overall orientation and tensile strength. The observed trends in tenacity, initial modulus, and high temperature shrinkage of the drawn/heat-set filaments appeared to be well correlated with the extent and distribution of amorphous phase rigidity as perceived through inferences made from the loss tangent temperature dependence. The WAXS patterns of the drawn/heat-set samples indicated that these filaments all possess a well-developed and highly oriented crystalline structure. Application of a simple two phase model allowed the determination of an amorphous orientation factor, which for the drawn/heat-set filaments was generally found to decrease as the draw ratio imposed in order to achieve comparable levels of elongation to break decreased. The SAXS patterns of the drawn/heat-set filaments indicated that comparable long period spacings exist in all cases and that a transition from a four-point pattern to a two-point bar-shaped pattern occurred when the precursor filament possessed some significant amount of as-spun crystallinity. J Appl Polym Sci 69: 2115–2131, 1998

Key words: take-up speed; properties; structure; as-spun filaments; drawn/heat-set filaments; poly(ethylene terephthalate)

INTRODUCTION

The strong impact of initial take-up speed on as-spun filament structure and properties has been recognized for a long time. During the early stages of this recognition it was hoped that fully oriented structures with properties approaching their theoretical maximum might be achieved through the use of ultrahigh take-up speeds. However, as engineering advancements made the utilization of these ultrahigh take-up speeds possible, the limited gain associated with this approach became evident. With the ultimate expectation laid to rest, the structure and properties changes that did occur through the use of these ultrahigh take-up speeds were still considered by many to be quite worthy of continued study.[1]

To develop the tensile strength, tensile modu-

Correspondence to: J. F. Hotter.

Journal of Applied Polymer Science, Vol. 69, 2115–2131 (1998)
 CCC 0021-8995/98/112115-17

lus, and dimensional stability necessary to make poly(ethylene terephthalate) (PET) filaments acceptable for industrial reinforcement type applications, the filaments were drawn up to 4 times their original length and subsequently heat-set. The drawing and heat-setting process is amenable to uninterrupted operation and can be performed on continuous filament at high speeds. The amount of draw imposed is usually set to achieve a desired level of elongation to break. Within this conventional procedure, the initial take-up speed prior to drawing has become an important process variable. Its importance stems from its ability to control the developing threadline stress and hence controlling the level of orientation and structure present in the as-spun material. In fact, many patents that deal with the melt spinning of PET filaments clearly identify the importance of this parameter and its significant effect on the properties of the drawn and heat-set filament product.[2–4]

The structure that develops during the initial spinning and the transformations that occur during the drawing and heat-setting stages are of obvious interest to both industry and academia, with many academic studies having been funded by the major synthetic filament producers of industry. While many of these studies have been limited to characterization of only the initial spinning process, some have gone to the next step and attempted to include the impact of varying as-spun structure on the drawn and heat-set filament structure and properties.[5–7] Another important facet of the need to understand the process–structure–property relationships present in PET filaments produced through conventional means is the background information this provides. Such background information can yield valuable insight when attempting to properly distinguish when a new process may or may not have created a new or unique product. In the present study, correlations and trends between initial take-up speed and a variety of key property and structural features of as-spun and drawn/heat-set PET filaments are discussed.

EXPERIMENTAL

Filament Spinning

A high molecular weight PET chip was used to produce all of the as-spun and drawn/heat-set filament samples. The intrinsic viscosity of the virgin chip was measured in a 60/40 wt % phenol/tetrachloroethane solution and is reported to be 0.97 dL/g. The filament was extruded from a single hole spinneret having an exit diameter of 0.6 mm. Figure 1 shows the experimental setup used in the preparation of as-spun and drawn/heat-set samples. The initial take-up speed was varied from 1250 to 5000 m/min at intervals of 1250 m/min. The polymer throughput was adjusted in conjunction with the initial take-up speed to achieve comparable linear densities of approximately 4.5 denier (d) in all of the drawn/heat-set filaments. The appropriate as-spun target denier for each take-up speed was estimated from prior knowledge of the ultimate behavior of each sample during the drawing process, which was generated through preliminary drawing trials. Each of the as-spun samples was then drawn

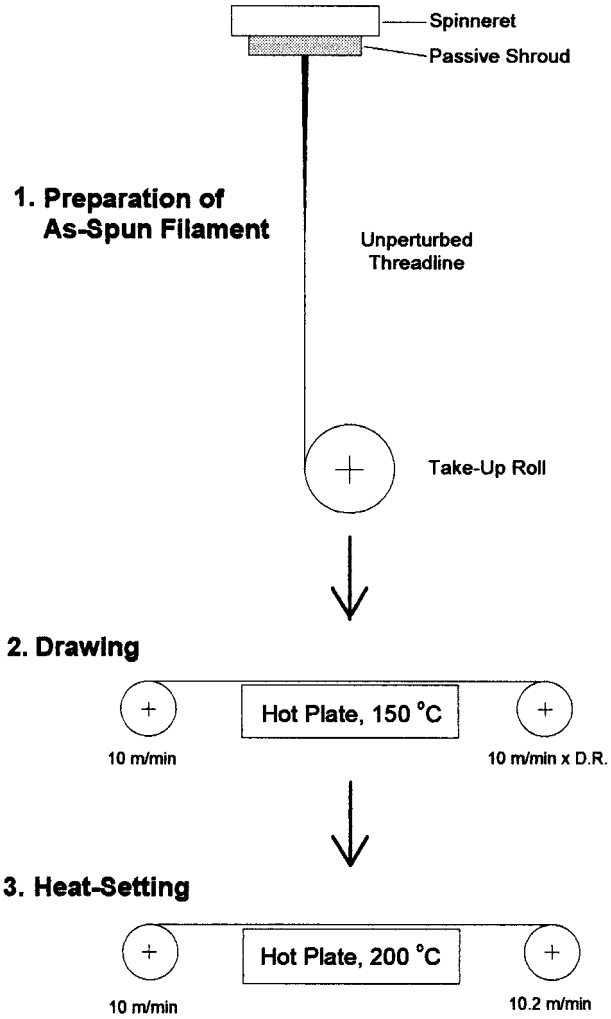

Figure 1 Experimental setup used in the preparation of as-spun and drawn/heat-set PET filaments.

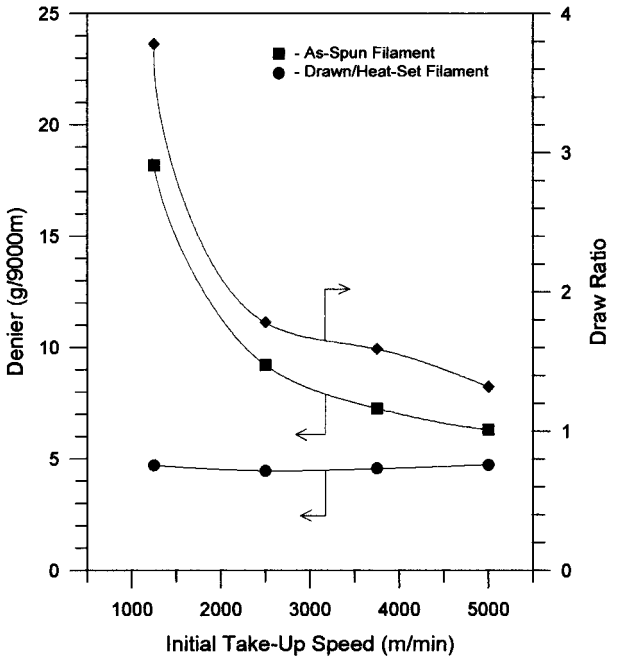

Figure 2 Denier and draw ratio as a function of initial take-up speed for as-spun and drawn/heat-set PET filaments.

to their near maximum draw ratio over a 30 cm long hot plate that was maintained at 150°C. These drawn filaments were subsequently heat set by passing them across the same 30 cm long hot plate that was now held at 200°C. As shown in Figure 1, the very minor difference in roll speeds (2%) indicates that this heat-setting process was conducted under an essentially constant length condition. While the residence time of the filament across the hot plate during the drawing process obviously varied with the imposed draw ratio, the subsequent heat-setting process did impose a relatively constant exposure time of approximately 1.8 s.

Figure 2 shows the as-spun and drawn/heat-set filament denier, as well as the imposed draw ratio as a function of initial take-up speed for all of the samples produced. The as-spun linear density varied from 18.2 d for the 1250 m/min case to 6.3 d for the 5000 m/min case. After drawing each of these samples to their near maximum, the resulting drawn/heat-set filament linear densities were all within the range of 4.48–4.75 d. The corresponding near maximum draw ratios ranged from 3.78 for the 1250 m/min case to 1.32 for the 5000 m/min case. As will be shown later, the imposed draw ratios also resulted in near equivalent elongation to break values in all of the drawn/heat-set samples. It is believed that the comparison of all other filament properties or characteristics among such a wide variety of initial spinning conditions is most appropriate when each of the posttreated filament samples possesses an equivalent level of elongation to break.

Filament Characterization

Crystallinity

Filament density was experimentally determined using a density gradient column according to ASTM D1505-68. Aqueous sodium bromide solution was used and maintained at 23 ± 0.1°C. Air bubbles were eliminated and wetability improved by centrifuging filament samples in solution prior to placement in the gradient column. Using glass reference beads of known density, an equation describing the linear density gradient within the column could be determined from regression analysis. From this equation the density of the filament samples was calculated from their equilibrium final resting position in the column. The measured density values were then converted to a volume fraction of crystallinity by simply interpolating between the densities of the completely amorphous and completely crystalline phases, as shown in eq. (1).

$$V_c = (\rho - \rho_a)/(\rho_c - \rho_a) \qquad (1)$$

Density values representative of the amorphous (ρ_a) and crystalline (ρ_c) phases were taken as 1.335 and 1.495 g/mL,[8] respectively.

Birefringence

A Jena interference microscope was used to characterize the filament samples. A zenon light source combined with an orange filter provided monochromatic illumination of 589-nm wavelength. A series of Cargille refractive index liquids were used to arrive at a retardation band displacement suitable for measurement. The mean birefringence (Δn) values were then calculated as follows:

$$\Delta n = n_{\parallel} - n_{\perp} \qquad (2)$$

Use of the interference technique for mean birefringence circumvented the problem associated with dispersion effects that becomes significant at high orders of retardation.

Tensile Properties

Mechanical properties were measured using a table model 1122 Instron tester. Properties to be reported include tenacity, elongation to break, initial modulus, and a stress amplification ratio (SAR). The SAR was calculated as the ratio of the secant modulus at 5% elongation to the initial modulus and provides a measure of the deviation from linearity that occurs just beyond the yield point. All calculations were performed in accord with ASTM D3822-82. All tests utilized single filaments of 25.4 mm gauge length. A constant rate of extension of 20 mm/min was imposed during all tensile tests. The values reported for each quantity represent the average of seven individual measurements.

Thermal Shrinkage

The measurement of boil-off shrinkage for select as-spun fibers was performed according to ASTM D2102-79. The measurement of free shrinkage at 177°C for select posttreated fibers was performed in accordance with ASTM D885-78. In either case the shrinkage was calculated as follows:

$$\text{shrinkage}\ (\%) = [(I - F)/I] \times 100 \qquad (3)$$

where I was the initial length of the specimen and F was the final length of the specimen.

Dynamic Mechanical Analysis

Dynamic mechanical measurements were performed on a Rheovibron model DDVII-C viscoelastometer manufactured by IMASS. In this test the ends of a 50-d filament bundle were mounted to opposing strain gauges using a gauge length of 20 mm. One end of the bundle was subjected to a sinusoidal tensile strain that resulted in a displaced sinusoidal stress at the other end of the sample. The phase angle between these two sinusoidal waves was monitored and reported as a tan δ value. The storage modulus, E', in phase with the imposed strain, and the loss modulus, E'', out of phase with the imposed strain, are related through the value of tan δ as follows:

$$\tan \delta = E''/E' \qquad (4)$$

The rheovibron was operated at a frequency of 11 Hz and at a scan rate of 2°C/min over the temperature range from 30 to 220°C. A fixed tension level of 0.25 gf/d was maintained on the sample during the test.

DSC

Thermal traces of the filament samples were conducted on a Perkin–Elmer series 7 thermal analysis differential scanning calorimeter interfaced to a Perkin–Elmer model 7700 professional computer. Samples weighing approximately 8 mg were scanned at 40°C/min over the range from 50 to 300°C. Filaments were cut such that small segments could be laid flat in the DSC sample pan. This method of sample preparation assured that no portion of the fibers were constrained, such as is the case with knotted samples. All scans were normalized to eliminate differences due to sample weight.

Wide-Angle (WAXS) and Small-Angle X-ray Scattering (SAXS)

A Siemens type-F X-ray diffractometer equipped with a nickel-filtered CuK_α radiation source and an evacuated camera (designed by W. O. Statton) was used to generate wide-angle flat plate photographs. The camera was set up using a pinhole collimator of 0.25 mm diameter and a sample to film distance of 8 cm.

The WAXS analysis was performed by the Allied-Signal Fibers Division using a Philips APD 1700 diffraction system in transmission mode with a CuK_α radiation source. The samples were mounted as a bundle of parallel filaments. Equatorial and meridional intensity scans were collected and profile fit using the appropriate number of Pearson VII functions.[9,10] The apparent lateral (010, 100) and longitudinal ($\bar{1}05$) crystallite dimensions were then calculated using the Scherrer equation,[11]

$$L_{hkl} = \frac{K\lambda}{\beta \cos \theta} \qquad (5)$$

where β is the peak halfwidth, K is taken to be unity, λ is the radiation wavelength, and θ is the Bragg angle. The crystallite orientation factor was determined using the Hermans function,

$$f_c = (3\langle \cos^2 \phi \rangle - 1)/2 \qquad (6)$$

where ϕ was taken as the full width at half maximum of the profile fit $\bar{1}05$ reflection generated from an azimuthal scan. The amorphous orienta-

tion factor was then calculated using the expression derived through the application of a simple two phase model as described by Stein and Norris,[12] which relates the overall measured filament birefringence (Δn) to the contributions from both the crystalline and amorphous phases.

$$\Delta n = f_c V_c \Delta n_c + f_a (1 - V_c) \Delta n_a \qquad (7)$$

where Δn_c and Δn_a represent the intrinsic birefringences of perfectly crystalline and amorphous PET, whose values were taken as 0.22 and 0.275,[13] respectively.

The SAXS analysis was performed at the Oak Ridge National Laboratory using a rotating anode CuK_α X-ray source, pinhole collimation (2 mm diameter at the sample), a sample to detector distance of 5 m, and a 2-dimensional position-sensitive detector with dimensions of 20 × 20 cm. The angular dimensions associated with the isointensity contour plots are in units of momentum transfer, Q, that is defined as

$$Q = (4\pi/\lambda)\sin(\theta_{scat}/2) \qquad (8)$$

The long period spacing (LPS) of the repeat lamellar structure was then calculated as

$$\mathrm{LPS} = 2\pi/Q \qquad (9)$$

where θ in eq. (8) is taken as the angular separation of the quadrant spots or meridional streaks in a direction parallel to the fiber axis.

RESULTS AND DISCUSSION

Crystallinity and Birefringence of As-Spun and Drawn/Heat-Set Filaments

Figure 3 shows volume fraction crystallinity and birefringence as a function of initial take-up speed for the as-spun and the drawn/heat-set filaments. The crystallinity and birefringence of the as-spun filaments both increase in a familiar well-established manner. The crystallinity remains essentially constant until the transition from 2500 to 3750 m/min, which is a range within which the onset of significant crystallization is known to occur, while the birefringence increases in a relatively linear fashion with increasing take-up speed. As for the drawn/heat-set filaments, it appears that both the crystallinity and birefringence varied only slightly as the initial take-up speed

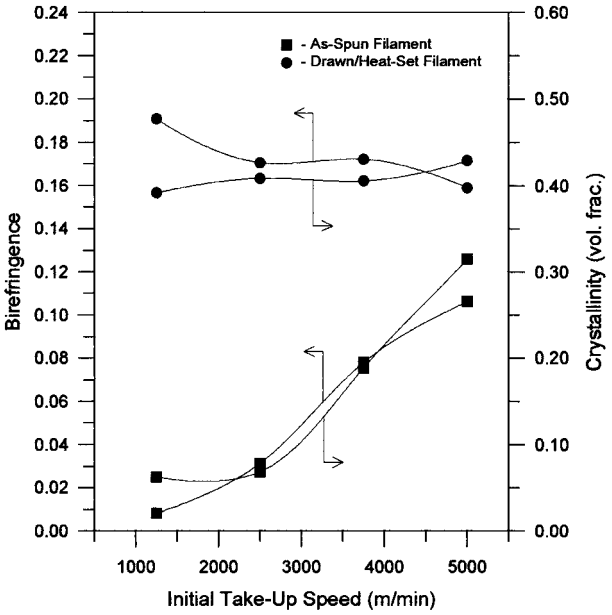

Figure 3 Birefringence and volume fraction crystallinity as a function of initial take-up speed for as-spun and drawn/heat-set PET filaments.

was increased. However, the trends observed in both cases are clear with a small but steady increase in crystallinity being accompanied by a slightly more pronounced decrease in birefringence.

The use of higher initial take-up speeds obviously induces significant structural development in the as-spun filaments. It is not unreasonable to assume that this preformed structure would have a significant impact or effect on the subsequent drawing and heat-setting process. Because one would expect the low speed spun, and most highly drawn and oriented filaments to achieve the highest level of crystallinity during the subsequent heat-setting process, the observed increase in drawn/heat-set filament crystallinity with increasing initial take-up speed (i.e., decreasing postdraw orientation) is not easily rationalized. It is believed that this may be an artifact of the time of exposure across the hot plate during the drawing process, and the filaments on which a lower draw ratio was imposed experienced a longer time of exposure at the elevated draw temperature. As for the progressive decline in birefringence, it is most likely the growing presence of crystallites acting as crosslinks that are limiting molecular rearrangement and the development of further orientation during the drawing process. According to Brody,[5] who properly recognized that high speed spun filaments are not like par-

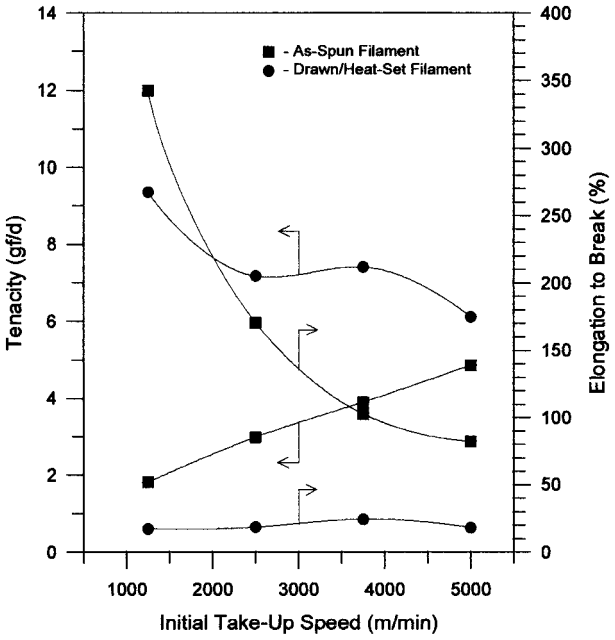

Figure 4 Tenacity and elongation to break as a function of initial take-up speed for as-spun and drawn/heat-set PET filaments.

tially drawn low speed spun filaments but are structurally different, deformation and heat treatment of both low and high speed spun PET filaments leads to an indistinguishable product. However, as shown in Figure 3, the obvious decline in birefringence for samples that have been drawn to very near the same final denier and elongation to break clearly shows that the inherent differences between low and high speed spun PET filaments are not completely erased during drawing and heat setting.

Tensile Properties of As-Spun and Drawn/Heat-Set Filaments

Figure 4 shows tenacity and elongation to break as a function of initial take-up speed for the as-spun and drawn/heat-set filaments. The tenacity of the as-spun filaments increases in a steady linear fashion from 1.82 gf/d at 1250 m/min to 4.87 gf/d at 5000 m/min, while the elongation to break decreases in a rapid exponential manner from 343% at 1250 m/min to 82% at 5000 m/min. Even though increasing take-up speeds move the tenacity and elongation to break values in the expected direction, the gap between as-spun and fully drawn properties remains unacceptably large. As shown in Figure 4, when the corresponding as-spun filaments are drawn to comparable levels of elongation to break (17–24%), the effect of initial take-up speed persists and continues to significantly impact the resulting tenacity. The effect is a reduction in tenacity of the drawn/heat-set filaments from 9.36 to 6.13 gf/d as the initial take-up speed was increased from 1250 to 5000 m/min, respectively. Figure 5 shows initial modulus and the previously defined SAR as a function of initial take-up speed for the as-spun and drawn/heat-set filaments. The initial modulus values of the as-spun filaments increase steadily with increasing take-up speed from 18.9 gf/d at 1250 m/min to 63.8 gf/d at 5000 m/min. The SAR values of the as-spun filaments, while more variable, decrease over this range of take-up speeds with values of 0.47 at 1250 m/min and 0.39 at 5000 m/min being observed. As for the drawn/heat-set filaments, the same general trends were observed with initial modulus and SAR values now ranging from 107.9 gf/d and 0.82 at 1250 m/min to 125.6 gf/d and 0.75 at 5000 m/min, respectively.

The behavior of tensile properties in polymeric filaments has often been used to make inferences regarding the structure of the load bearing segments or regions within the filament. Consider first the key components of any structural model of a semicrystalline polymeric material: the crystalline and amorphous phases. The crystalline phase is generally believed to be present as rigid

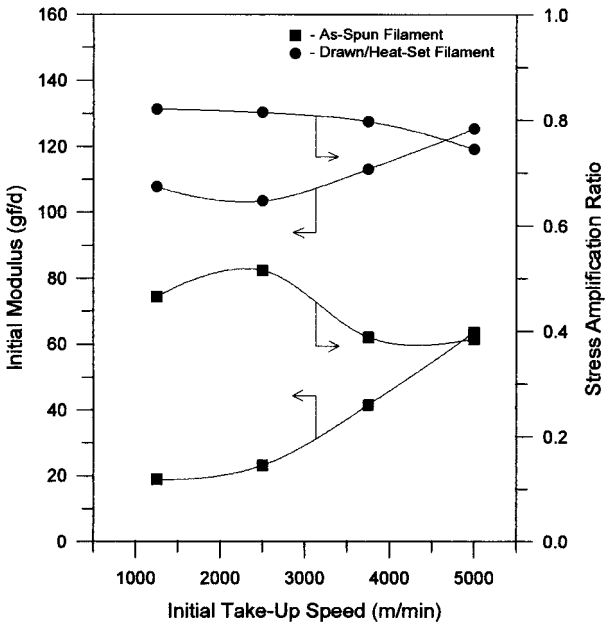

Figure 5 Initial modulus and stress amplification ratio as a function of initial take-up speed for as-spun and drawn/heat-set PET filaments.

blocks that are dispersed within a surrounding mass or phase of less oriented amorphous material. These rigid blocks act in essence as crosslinks and help to provide a greater level of connectivity within the structure as a whole. Because the modulus of a PET crystal lies approximately an order of magnitude greater than the modulus of any PET filament ever produced, it is widely accepted that it is primarily the structure of the amorphous regions that controls the strength and stiffness of actual semicrystalline filaments.[14,15] The molecular chains within the amorphous regions that successfully traverse the distance between crystalline blocks, and hence connect them, are usually described as "tie molecules." It is then the number and distribution of lengths of these tie molecules that will control to a great extent the load bearing behavior of the filament. For the as-spun filaments it may merely be the significant increase in crystallinity or number of crystalline blocks, which leads to the observed increase in all of the as-spun tensile properties. However, for the drawn/heat-set filaments the crystallinity is not so variable that such a simple explanation should suffice. It is believed that for the drawn/heat-set filaments the decrease in tenacity and increase in modulus that correspondingly occur as the initial take-up speed increases are indeed due to variations in either the number or the distribution of lengths associated with the tie molecules or both of them. If it were assumed for simplicity that an equivalent number of tie molecules existed within all of the draw/heat-set filaments, then the observed balance between tenacity and modulus may be the result of an increase in the number of relatively more taut tie chains in the filaments produced at the higher initial take-up speeds. The argument being that the greater number of taut tie chains would increase the initial modulus, while the fewer number of tie chains of average length, which dictate the overall strength, would decrease the tenacity. The potential for a distorted or skewed distribution of tie chain lengths to alter the balance among tensile properties stems from the inhomogeneous manner in which stress is forced to develop among the connecting tie chains.[16] This type of distorted or skewed distribution of tie chain lengths might also lead to the increased deviation from linearity in the stress–strain behavior as indicated by the declining SAR values. However, until more powerful means of characterizing the amorphous regions are developed, the explanation offered here must be considered speculative.

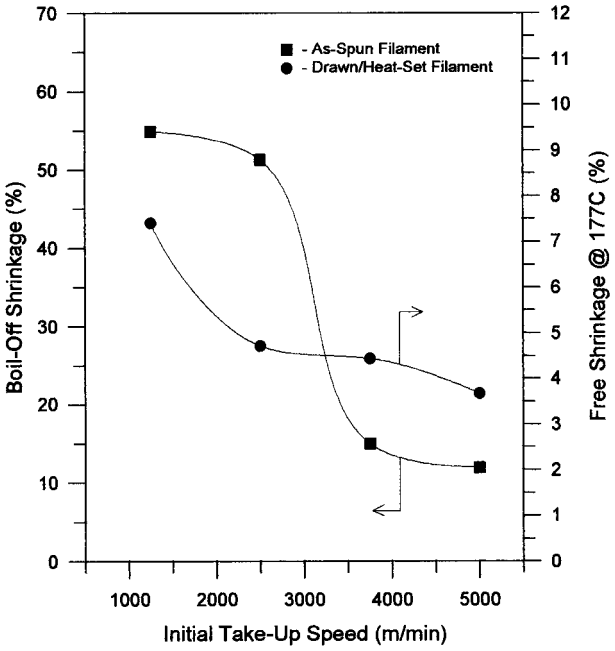

Figure 6 Boil-off shrinkage and free shrinkage at 177°C as a function of initial take-up speed for as-spun and drawn/heat-set PET filaments.

Thermal Analysis of As-Spun and Drawn/Heat-Set Filaments

Figure 6 shows both boil-off shrinkage of the as-spun filaments and free shrinkage at 177°C of the drawn/heat-set filaments as a function of initial take-up speed. The boil-off shrinkage decreases dramatically as the initial take-up speeds exceed 2500 m/min and then levels off. This reduction in shrinkage is attributed to the onset of stress-induced crystallization. As for the leveling off effect, even though the continued increase in crystallinity over the 3750–5000 m/min range is significant, it occurs primarily in the form of larger crystallites, as opposed to a greater number of them. Hence, the number of effective crosslinks has not increased in the same proportion as the overall volume fraction crystallinity. All of the drawn/heat-set filaments possess crystallinities that vary to a much lesser extent. Hence, the higher temperature free shrinkages also vary much less than the observed boil-off shrinkages. As shown in Figure 6, a clear trend emerged with free shrinkage of the drawn/heat-set filaments decreasing as the initial take-up speed was increased. While the level of crystallinity present plays an important role in determining the shrinkage behavior, just as important, if not more so, is the characteristic state of the amorphous

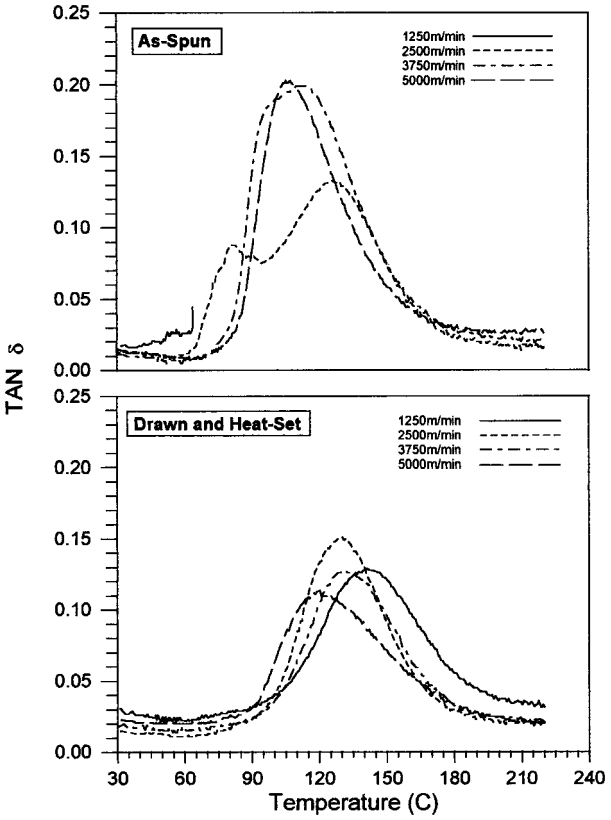

Figure 7 Loss tangent as a function of temperature for as-spun and drawn/heat-set PET filaments.

phase. The shrinkage behavior of annealed or heat-set filaments has been shown to correlate well with the orientation of the amorphous regions[17] with higher amorphous orientation giving rise to a greater propensity to shrink or change dimensions as elevated temperatures increase chain mobility within the amorphous regions. In accord with the expression used by Stein and Norris[18] for determining the amorphous orientation, if the crystallites in each of the samples are well oriented and all possess comparable levels of crystallinity, the amorphous orientation will vary in the same manner as the overall orientation or birefringence. As shown later, this is indeed the case and the observed shrinkage behavior of the drawn/heat-set filaments is in good agreement with that expected based on the declining birefringence and amorphous orientation.

Figure 7 shows the loss tangent as a function of temperature for the as-spun and drawn/heat-set filaments. In the as-spun filaments, the most unusual features are those associated with the low speed spun filaments. Data collection for the 1250 m/min sample was terminated very early in the scan due to excessive elongation during cyclic loading as the temperature was increased. In the 2500 m/min sample, the appearance of twin peaks clearly indicates the occurrence of structural changes during the temperature scanning process. As with any high temperature characterization technique that is performed on as-spun filaments, inevitable structural changes occur during the scanning process. While much useful information regarding the original structure can still be learned from the results of such tests, caution must be exercised in their interpretation. The most distinctive feature between the samples spun at the higher speeds is a significant reduction in the breadth of the observed loss tangent peak for the 5000 m/min sample. The only feature among all of the as-spun samples that is likely the least disturbed by the annealing that occurs during the test procedure is the temperature that corresponds to the maximum slope experienced during the onset of the α transition, which is sometimes taken to represent the glass transition.[19] As shown in Figure 7, when evaluated in this manner the glass transition temperature increased as the initial take-up speed was increased. Consider now the loss tangent response shown in Figure 7 for the drawn/heat-set filaments. In general, the peak intensity and corresponding peak temperatures were both depressed as the initial take-up speed was increased. A narrowing or decrease in breadth of the loss tangent peaks was also observed as the initial take-up speed was increased. As with all of the previously discussed drawn/heat-set filament properties, the loss tangent behavior observed here appears to also be controlled to some extent by the structure set by the initial take-up speed.

The dynamic loss tangent has been previously defined as the ratio between the loss and storage moduli. On a fundamental basis, the loss tangent represents the fraction of energy lost per cycle due to viscous dissipation caused by friction between molecules during chain segment motion. However, a number of other insightful connotations have also been adopted. Murayama[20] refers to the loss tangent in general terms as a type of internal friction, Kamide et al.[7,21] considers the loss tangent to be a direct means of probing the packing density of the amorphous regions, and Takayanagi and Matsuo[22,23] propose interpretations based on relaxation time spectra. The loss tangent is typically tracked as a function of temperature, and the largest peak, usually referred to as the α transition, occurs within the glass transition

region. As described by Murayama,[20] this transition occurs in the amorphous regions of the polymer with the initiation of micro-Brownian motion of molecular chains. Murayama[20] further expounded on his interpretation of this transition with claims that both the magnitude and peak temperature of the transition can be considered as characteristic parameters that provide insight as to the amount of amorphous material present and the rigidness with which it is held, respectively. The types of structural features that could give rise to such variations in amorphous phase rigidity are typically associated with the existence and extent of any physical constraints that might be imposed on the chain segments, such as those due possibly to an increased packing density, entanglements, or crystallites that could act as crosslinks in semicrystalline materials. In fact, Murayama[20] also recognized the potential for the size and manner of distribution of such crystallites to significantly influence the extent of chain segment mobility, and thus impact the transition peak temperature, as well as the breadth of the peak. The significance of the peak breadth is usually taken as an indication of the extent of variability in amorphous phase mobility or packing density.

Consider now how this background information can be of assistance in interpreting the loss tangent behavior of the filaments of the present study. As described previously, the as-spun filament produced at the lowest take-up speed of 1250 m/min could not be tested in this manner due to excessive elongation, which was clearly due to the poor load bearing capability of the unoriented amorphous type of structure that it possesses. The as-spun filament produced at 2500 m/min obviously incurred significant structural changes during the test. These structural changes were a result of the orienting elongation and annealing that occurred during the test. The as-spun filaments produced at the higher take-up speeds, while still susceptible to structural changes, already possess a partially developed structure and appear to yield some valid information regarding the initial structure. If this is indeed the case, and the transition attributes of the two as-spun filaments produced at the higher take-up speeds can be compared to one another, the most apparent difference is the reduction in peak breadth as the initial take-up speed was increased from 3750 to 5000 m/min. This reduction in peak breadth indicates that less variability is present in the extent of chain mobility within the amorphous phase, which is likely due to the continued increase in crystallinity. In the case of the drawn/heat-set filaments, each of these samples has a comparable heat history and well-developed structure; hence, any changes resulting from annealing during the test are minimized and direct comparisons between samples are considered much more valid. In terms of general trends, the peak magnitude and temperature of the observed transitions both decreased as the initial take-up speed was increased. This suggests that the amorphous fraction or content decreased while amorphous mobility increased as the initial take-up speed was increased. The only significant discrepancy present within these general trends is in the magnitude of the peak of the 1250 m/min sample. Based on its slightly lower crystallinity, this filament presumably possesses a higher fraction of amorphous material, which should result in a transition peak of greater magnitude. However, it must also be kept in mind that severe enough constraints to chain movement, such as in taut tie molecules, could force some amorphous chain segments to behave more like the rigidly held chain segments of the crystalline phase. Hence, this discrepancy could be the result of a shift in the balance between an increasing fraction of the amorphous phase that would increase the magnitude of the peak and a greater severity of imposed constraints to chain movement that would decrease the magnitude of the peak. The breadth of each peak in the drawn/heat-set filaments also appears to be controlled to some extent by the initial take-up speed. The breadth of each peak decreased as the take-up speed was increased from 1250 to 3750 m/min, indicating a decrease in the variability of chain segment mobility within the amorphous regions. As for the filament produced at 5000 m/min, its transition peak appears to have begun to broaden in a slightly asymmetric manner, which could be considered supportive of the previous hypothesis regarding the existence of a distorted or skewed distribution of tie chain lengths within this sample. Due to the fact that constraints to chain segment mobility can result from either, or both, an increase in the general packing density, which may contribute relatively little to the load bearing capability of the structure, or an increase in the number and length distribution of so-called tie molecules, which likely contributes significantly to the load bearing capability of the structure, it is not considered appropriate to attempt to correlate the observed

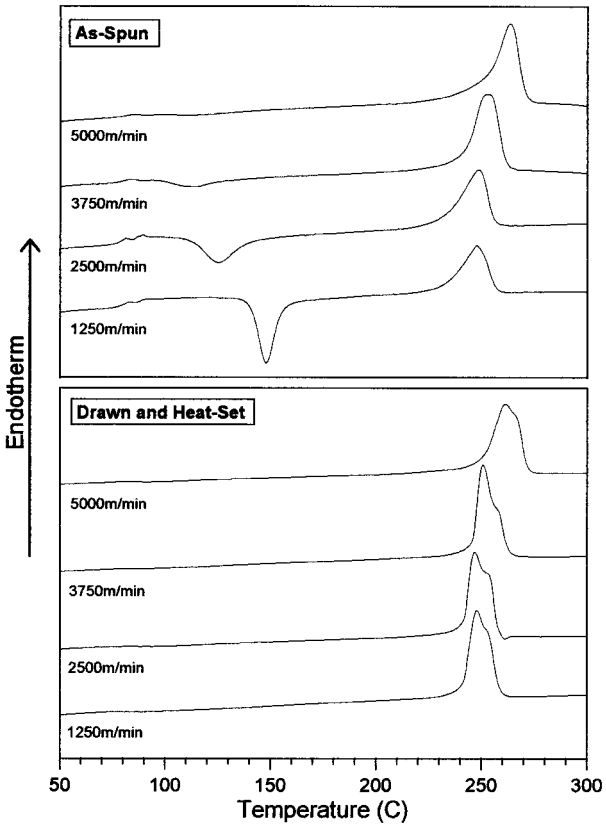

Figure 8 DSC traces of as-spun and drawn/heat-set PET filaments (scan rate = 40°C/min).

characteristics of these α transitions to the corresponding tensile properties of the filaments.

Figure 8 shows the DSC traces of the as-spun and drawn/heat-set filaments for each take-up speed. In the as-spun filaments the magnitude of the glass transition and the crystallization exotherm decrease with increasing take-up speed, almost to the extent that neither can be distinguished in the filament produced at 5000 m/min. The peak temperatures of the corresponding melting endotherms increase with increasing take-up speed. As for the drawn/heat-set filaments, none of these filaments exhibits a clearly distinguishable glass transition or crystallization exotherm. The peak temperature of the melting endotherms of all of the drawn/heat-set filaments increased with increasing take-up speed, as was also the case in the precursor as-spun filaments. However, now each of the melting endotherms display what appear to be dual overlapping peaks.

The characteristic features of DSC traces are generally the temperature and magnitude associated with the glass transition, the crystallization exotherm, and the melting endotherm. The glass transition represents the onset of rotational and translational molecular motion within the noncrystalline (amorphous) phase and is characterized by an increase in heat capacity as the temperature is increased. Wunderlich et al.[19,24] discussed the possibility of the magnitude of the change in heat capacity being affected by rigidity of the amorphous phase, with a more rigid amorphous phase reducing the magnitude of the change in heat capacity. As the change in heat capacity becomes minimal, the accurate identification of the glass transition temperature can become difficult. The crystallization exotherm occurs as a result of thermally induced crystallization which takes place during the DSC heating process. As described previously, this can result in structural changes during the test procedure that confound information regarding the initial structure. The melting endotherm is associated with the melting of the crystalline phase. Shimizu[25] showed a correspondence between higher melting peak temperatures and the presence of large crystallites and an oriented superstructure. The area or magnitude of the melting endotherm is often taken as an indication of the amount of the crystalline phase present. The appearance of multiple overlapping melting endotherms has also been discussed at length in the appropriate literature, and two separate interpretations emerged. The earliest of these interpretations attributed the appearance of dual peaks to the existence of two separate crystal morphologies, such as folded versus partially extended chain structures[26,27]; the later interpretation more simply attributed the second higher temperature peak to a recrystallization phenomenon.[28,29]

The glass transition temperatures of the as-spun filaments are well defined and all occur at approximately 80°C. However, the magnitude of the change in heat capacity consistently decreased, indicating that a more rigid amorphous phase developed in the as-spun filaments as the initial take-up speed was increased. Also, as the take-up speed was increased, the crystallization exotherms moved to lower temperatures due to an increased level of orientation and decreased in magnitude due to a more well-developed as-spun crystalline structure. As for the melting endotherms, the as-spun filaments produced at the lower take-up speeds of 1250 and 2500 m/min are known to possess a relatively small fraction of the crystalline phase. Hence, their melting endotherms are simply considered to be a result of the crystallization that takes place during the test

procedure and not representative of a fraction of the crystalline phase present in the as-spun filament. The as-spun filaments produced at the higher take-up speeds of 3750 and 5000 m/min already possess a partially developed structure; hence, these melting endotherms are presumed to better represent true features of the initial as-spun structure, and the increase in melting point indicates the development of larger, more perfected, crystallites as the take-up speed was increased. As for the drawn/heat-set filaments, all of the samples exhibit only a minor increase in heat capacity that occurs in a very gradual manner that results in a poorly defined and very broad glass transition. Although according to Wunderlich et al.[19,24] this indicates that similar levels of rigidity exist in the amorphous phase of each of these samples, the previously discussed loss tangent behavior contradicts this notion. Therefore, it must be concluded that DSC characterization lacks the sensitivity required to probe, in any great detail, the structure of the amorphous phase, especially in highly crystalline and ordered structures. Due to their well-defined structures, the lack of a crystallization exotherm in any of the drawn/heat-set filaments is not unexpected. The peak temperature of the melting endotherms observed in the drawn/heat-set filaments correspond well with their respective as-spun precursors. This suggests that the nature of the crystallites formed, or not formed, in the as-spun filament significantly impact the resulting melting point observed in the drawn/heat-set filaments. Consider finally the consistent presence of the apparent dual melting peaks in all of the drawn/heat-set filaments. The fact that dual peaks appear regardless of the as-spun structure leads to the conclusion that this feature develops as either a consequence of changes incurred during post-treatment or due to the previously mentioned recrystallization phenomenon. Because all of the drawn/heat-set filaments have well-developed structures and a relatively rapid scan rate of 40°C/min was imposed, the occurrence or extent of any recrystallization is considered to have been minimal. Hence, it is believed that the higher temperature peaks are the result of larger more perfect crystallites or portions of crystallites that are formed during the spinning and/or drawing processes, while the lower temperature peaks are possibly the result of some type of less perfect epitaxial overgrowth that occurs during the heat-setting or scanning process on the surfaces of the crystallites already present.[5] The concept of a lower temperature melting peak being attributed to a structure, such as that suggested, formed during heat-setting or annealing was reported previously by Nealy et al.[30]

X-Ray Analysis of As-Spun and Drawn/Heat-Set Filaments

Figure 9 shows the WAXS patterns of the as-spun and drawn/heat-set filaments for each take-up speed. The as-spun filament produced at 1250 m/min exhibits a strong uniformly distributed amorphous halo. As the take-up speed was increased to 2500 m/min, the amorphous halo has begun to concentrate along the equator. At the take-up speed of 3750 m/min, distinct reflections are now present along the equator; at 5000 m/min, the intensity of these equatorial reflections has become even stronger, and other off-equator reflections have become more well defined. The patterns of the drawn/heat-set filaments produced from each of these precursor samples all appear very similar and are indicative of well-defined and highly oriented crystalline structures. In an attempt to more accurately identify discriminating features among the crystalline structures in both the as-spun and drawn/heat-set filaments, intensity scans of various crystallite reflections were generated and analyzed in accord with the procedure described earlier to yield quantitative estimates of crystallite dimensions and orientation factors, the results of which are presented in Table I. The following discussion will utilize the WAXS patterns as a qualitative tool for discussing general features and then refer to the experimentally derived crystallite dimensions and orientation factors when a greater level of detail is required.

The general features considered to be of prime importance in the interpretation of WAXS patterns are the presence (or lack thereof) of scattering from amorphous and crystalline components, as well as their corresponding intensity distributions. In simple terms, the quantity present of a particular component or phase can be gauged through its corresponding intensity; the shape of the intensity distribution provides an indication of the size, perfection, and orientation of the component responsible for the scattering. The concentration of amorphous phase scattering along the equator present in the as-spun filament produced at 2500 m/min has been observed previously[31] and is taken as an indication of an overall increase in chain alignment along the filament axis. The

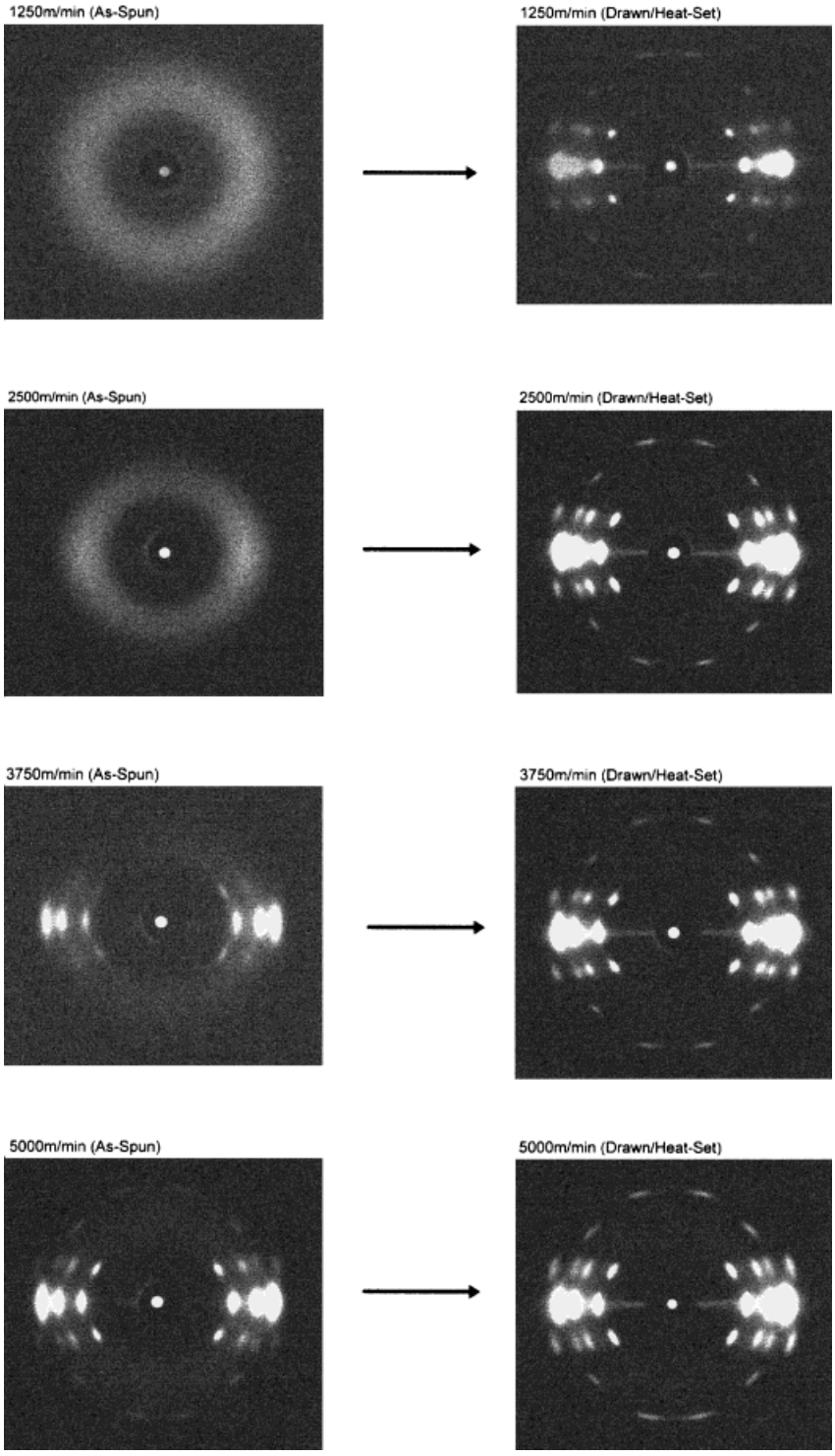

Figure 9 WAXS patterns of as-spun and drawn/heat-set PET filaments.

strong equatorial reflections present in the as-spun filament produced at 3750 m/min indicate the development of significant crystallization during the spinning process and corresponds well with the substantial increase in percent crystallinity that was also observed at this take-up speed. The greater intensity of the equatorial reflections, as well as the emerging off-equator re-

Table I Crystallite Dimensions, Orientation Factors, and Long Period Spacings (LPS) of As-Spun and Drawn/Heat-Set PET Filaments

Sample Identification	010 (Å)	100 (Å)	$\bar{1}05$ (Å)	f_c	f_a	LPS (Å)
1250 m/min (as spun)	—	—	—	—	—	—
2500 m/min (as spun)	—	—	—	—	—	—
3750 m/min (as spun)	36	48	54	0.971	0.169	—
5000 m/min (as spun)	61	56	103	0.976	0.205	—
1250 m/min (drawn/heat set)	56	45	89	0.981	0.637	151
2500 m/min (drawn/heat set)	74	53	90	0.985	0.505	152
3750 m/min (drawn/heat set)	72	52	89	0.984	0.517	152
5000 m/min (drawn/heat set)	78	61	94	0.985	0.422	162

flections present in the as-spun filament produced at 5000 m/min, indicate increases in the amount and perfection of the crystalline material present. With the onset of a well-developed crystalline structure, such as that present in the as-spun samples produced at the higher initial take-up speeds, comes the ability to quantitatively estimate crystallite dimensions and orientation factors. As shown in Table I, the crystallite dimensions nearly doubled in both the lateral and longitudinal directions as the initial take-up speed was increased from 3750 to 5000 m/min. As also shown in Table I, while the crystallite orientation factor remained essentially constant at approximately 0.97, the amorphous orientation factor increased from 0.169 to 0.205 as the initial take-up speed was increased from 3750 to 5000 m/min. The WAXS patterns of each of the drawn/heat-set filaments qualitatively indicate the presence of a well-developed and highly oriented crystalline structure. This qualitative interpretation is further substantiated by the corresponding crystallite dimension and orientation factor data presented in Table I. Upon closer examination of the data shown in Table I, there also appears to be a slight increase in the lateral crystallite dimensions (010, 100) as the initial take-up speed was increased, while the longitudinal dimension ($\bar{1}05$) remained essentially constant at approximately 90 Å. As for the orientation factors of the drawn/heat-set filaments, the crystallite orientation factor was very high and also remained essentially constant at approximately 0.98, whereas the amorphous orientation factor showed a steady decline from 0.637 to 0.422 as the initial take-up speed was increased from 1250 to 5000 m/min. This decline in amorphous orientation is attributed primarily to the much reduced draw ratio that could be achieved during posttreatment in the as-spun filaments produced at the higher initial take-up speeds. Note that as would be expected, the decline in amorphous orientation correlates well with the previously described decline in drawn/heat-set filament tenacity and shrinkage.

Figure 10 shows the SAXS patterns of the as-spun and drawn/heat-set filaments for each take-up speed. The as-spun filaments produced at 1250 and 2500 m/min exhibit incoherent (nonperiodic) scattering elongated along the equator, as well as the typical scatter observed around the beam stop. As shown in the SAXS patterns of the 3750 and 5000 m/min samples, as the take-up speed was increased further, the incoherent scattering along the equator was accompanied by the development of significant scattering that occurred in an $\times$ or cross-shaped pattern. As also observed in the WAXS patterns, the SAXS patterns of the drawn/heat-set filaments produced from each of these precursor samples show much less distinction between each other. All of the drawn/heat-set filaments continue to exhibit incoherent scattering along the equator. However, now each of these filaments also exhibit some level of coherent (periodic) scattering along the meridian; the general shape of the scattering appears as a bar or streak perpendicular to the fiber axis that is oriented in the vertical direction. Upon close examination, the bar-shaped patterns present in the drawn/heat-set filaments produced at the lower initial take-up speeds of 1250 and 2500 m/min split into what is usually referred to as a four-point or four-lobe pattern. As for the drawn/heat-set filaments produced at the higher initial take-up speeds of 3750 and 5000 m/min, there is no discernible separation and a simple two-point bar-shaped pattern exists. The determination of a longitudinal LPS requires

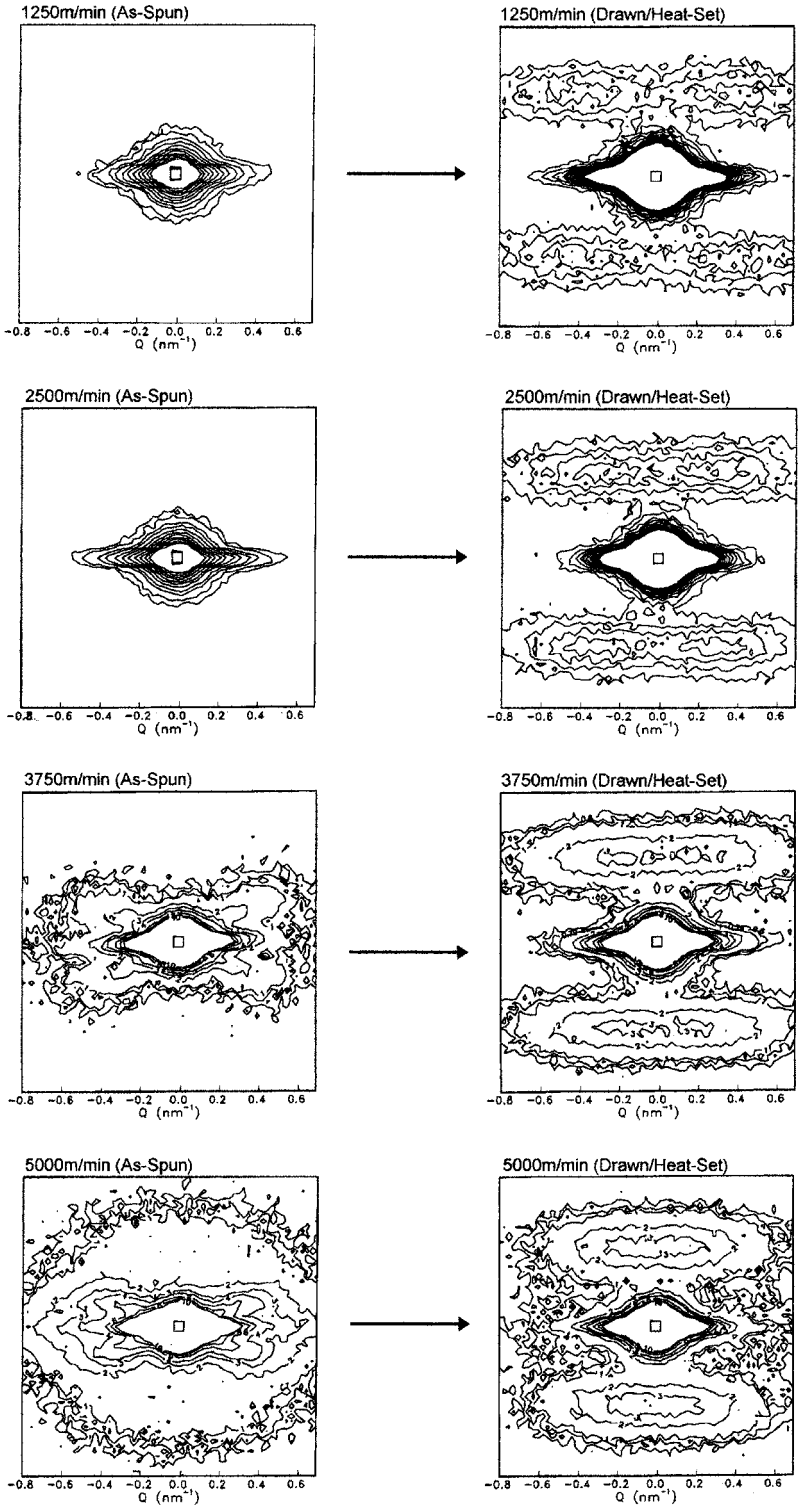

Figure 10 SAXS patterns in isointensity contour plot format of as-spun and drawn/heat-set PET filaments.

well-defined maxima along the meridional direction; hence, this quantity could be determined only for the drawn/heat-set filaments, the values for which are shown in Table I.

The scattering of X rays at small angles is attributed to fluctuations in electron density. If such fluctuations occur in a regular or periodic manner, the scattering intensity will develop well-defined maxima in the direction of the periodicity and the location of the maxima will provide a physical estimate of the linear dimension of this periodicity. Consider first the equatorial scattering that occurs in all of the as-spun and drawn/heat-set filaments. The presence of equatorial scattering indicates that a detectable variation in electron density exists in the direction perpendicular to the fiber axis, while its incoherence implies that the density modulation is not regular or periodic in nature. Some researchers focused on extracting the transverse dimension of fibrils, which are believed to be present as part of the microstructure, from equatorial slices of intensity versus scattering angle.[31] Others suggested that the diffuse equatorial scattering more likely represents the scattering from microvoids that exist in between microfibrils.[32,33] Yet another proposed explanation describes a structure that possesses less discrete internal boundaries and is considered to be better described as an interpenetrating set of molecules networked together by entanglements and microcrystals. From this perspective, the incoherent equatorial scattering is attributed to highly anisotropic planes of poor network connections (i.e., microcracks or microvoids) that are oriented parallel to and radially symmetric around the fiber axis.[34] In the present study, the occurrence of equatorial scattering appears to be significant even in the as-spun filaments produced at the lower initial take-up speeds, which are not highly suspect of containing any significant percentage by volume of anisotropic microvoids. Thus, while the general equatorial scattering shown in all of the SAXS patterns of Figure 10 is considered to represent an actual nonperiodic density fluctuation in a direction transverse to the fiber axis, the principal source of this fluctuation is not considered to be the presence of microvoids. In fact, if the notion of a microfibril is correct, it may simply be some type of less dense interfibrillar amorphous region that gives rise to a radial fluctuation of electron density, which also happens to be rendered nonperiodic by the development of microfibrils that may be cylindrical but not strictly round in cross section. Note that the proposed evidence for the existence of an interfibrillar phase has been suggested within numerous studies.[35–39] However, the lack of any regular periodicity being observed in the direction perpendicular to the fiber axis has been a stumbling block to the widespread acceptance of this proposed discernible phase. As for the cross-shaped wings that appear in the SAXS patterns of the as-spun filaments produced at 3750 and 5000 m/min, this has been attributed to a larger longitudinal periodicity buried by beam stop scattering and/or an inclination with respect to the filament axis of the source of the electron density fluctuation.[33] It should also be noted that nonmeridian radial-type scattering has been associated with crystallites that exist in a form that more closely resembles a lamellae structure than a fibrillar structure.[40] Consider now the coherent meridional scattering that occurs only in the drawn/heat-set filaments. The four-point pattern occurring in the highly drawn samples that were spun at the two lowest initial take-up speeds of 1250 and 2500 m/min is usually associated with one of two possible structures that could theoretically give rise to the observed patterns. The first of these is a structure in which the crystallites and hence the constituent molecular chains are both tilted with respect to the filament axis. The second of these is a structure in which only the apparent face of the crystallites is slanted, possibly as the result of an intensive internal shear stress caused by the large imposed draw ratio, while the constituent molecular chains in this case remain well oriented and relatively parallel to the filament axis. In light of the high levels of birefringence and crystallite orientation of these samples, the latter of these possible structural representations is believed to be the more realistic description. As for the two-point or bar-shaped pattern that occurred in the less highly drawn samples produced at the higher initial take-up speeds of 3750 and 5000 m/min, these are indicative of a 1-dimensional array of cylindrical scattering objects arranged parallel to the filament axis. While the range of features present in the resulting SAXS patterns of the drawn/heat-set filaments suggest that the shape and/or dimension of the crystallites may vary, all of the patterns indicate the existence of a long-range periodicity along the direction of the filament axis. As shown in Table I, the linear dimension of this LPS was essentially constant at 152 Å in all of the drawn/heat-set filaments, except for the sample produced at the highest initial take-up speed of 5000 m/min, which yielded an LPS of 162 Å. In

accord with previous interpretations, the appearance of each of these SAXS meridional scattering maxima is attributed to the longitudinal arrangement of alternating crystalline and amorphous regions.

SUMMARY AND CONCLUSIONS

Significant increases in the orientation, crystallinity, and tensile properties of the as-spun filaments occurred as the initial take-up speed was increased. Unfortunately, these increases reach their maximum well below the range required for direct use in any type of reinforcement application. Hence, almost all PET industrial filament spinning processes incorporate some degree of posttreatment. As the level of orientation and crystallinity increase with increasing initial take-up speed, the postspinning draw ratio required to achieve comparable elongation to break values decreases. However, two of the key properties that we usually attempt to maximize (i.e., tenacity and modulus) typically respond in an opposing manner. As as-spun orientation and crystallinity increase, the tenacity that can be achieved in the drawn/heat-set filament decreases and the modulus increases.

Thermal analysis of the as-spun and drawn/heat-set filaments was performed via the measurement of high temperature shrinkage, loss tangent temperature dependence, and DSC melting behavior. The shrinkage, or propensity to change dimension, was found to decrease in the as-spun and drawn/heat-set filaments as the initial take-up speed was increased. The observed shrinkage response is considered to have been dominated by increasing crystallinity for the as-spun filaments and decreasing amorphous orientation for the drawn/heat-set filaments. The loss tangent behavior clearly identified differences in the amorphous phase fine structure of the drawn/heat-set filaments. The changes in magnitude and position of the loss tangent peak indicate that the relative amount of amorphous material present decreased while the extent of its mobility increased as the initial take-up speed was increased. The observed melting point in the as-spun and drawn/heat-set filaments increased with increasing initial take-up speed. The fact that only the drawn/heat-set filaments display melting endotherms composed of apparent dual overlapping peaks is considered evidence in favor of the lower temperature peak being directly attributable to the formation of smaller crystallites and/or the presence of some type of less perfected overgrowth on existing crystallites that develops during posttreatment.

The structural detail of the as-spun and drawn/heat-set filaments has also been investigated through the qualitative inspection of WAXS and SAXS patterns, the quantitative evaluation of lateral and longitudinal crystallite dimensions, and the determination of crystalline and amorphous orientation factors. It was found that discernible crystallite reflections begin to appear in the as-spun filaments somewhere between initial take-up speeds of 2500 and 3750 m/min, which corresponds well with the rapid increase in percent crystallinity via density also observed. However, the development of well-defined longitudinal long-range periodicity, (i.e., the regular spacing of alternating crystalline and amorphous regions in the direction parallel to the filament axis) does not occur in any of the as-spun filaments, even for the filament produced at the highest initial take-up speed of 5000 m/min. WAXS patterns of the drawn/heat-set samples indicate that all of these filaments possess well-defined and highly oriented crystalline structures. Application of a simple two phase model allowed the determination of an amorphous orientation factor, which increased with increasing take-up speed in the as-spun filaments, and then decreased with increasing take-up speed (i.e. lower imposed postspinning draw ratio) in the drawn/heat-set filaments. The corresponding SAXS patterns of the drawn/heat-set samples indicate that all of these filaments possess LPSs of comparable dimension ranging from 151 to 162 Å. The SAXS patterns also indicate that the crystalline–amorphous phase boundary or interface present in the more highly drawn filaments, which were produced at the lower initial take-up speeds, appear to have a skewed or tilted texture along the exterior surface whose plane normal lies in the general direction of the filament axis. This skewed interface is believed to be a consequence of the greater extent of internal shear experienced within these filaments as a direct result of the larger imposed draw ratios.

In conclusion, a comprehensive study of the effect of initial take-up speed on the properties and structure of as-spun and drawn/heat-set PET filaments was performed. Although the significance of the effects of initial take-up speed on the as-spun properties and structure is well known, its impact on the drawn/heat-set filament product has not yet been well documented. The results

presented here clearly demonstrated that a wide range of drawn/heat-set filament properties can be achieved through the control of as-spun filament structure via initial take-up speed. In light of the increasing demand for specifically tailored property balances in filaments or fibers for industrial and textile applications, the manipulation of this critical process variable will surely continue to play an important role.

REFERENCES

1. A. Ziabicki and H. Kawai, Eds., *High-Speed Fiber Spinning,* Interscience, New York, 1985.
2. E. I. Du Pont de Nemours and Co., U.S. Pat. 5,034,182 (1991).
3. Allied-Signal, U.S. Pat. 5,067,538 (1991).
4. Fiber Industries, Inc., U.S. Pat. 4,414,169 (1983).
5. H. Brody, *J. Macromol. Sci., Phys.,* **B22,** 407 (1983).
6. A. Hamidi, A. S. Abhiraman, and P. Asher, *J. Appl. Polym. Sci.,* **28,** 567 (1983).
7. K. Kamide, T. Kuriki, and S. Manabe, *Polymer,* **18,** 163 (1986).
8. P. B. Rim and C. J. Nelson, *J. Appl. Polym. Sci.,* **42,** 1807 (1991).
9. H. M. Heuvel, R. Huisman, and K. C. J. B. Lind, *J. Polym. Sci., Polym. Phys. Ed.,* **14,** 921 (1976).
10. R. Huisman and H. M. Heuvel, *J. Polym. Sci., Polym. Phys. Ed.,* **14,** 941 (1976).
11. P. Scherrer, *Gottingher Nachrichten,* **2,** 98 (1918).
12. R. S. Stein and F. H. Norris, *J. Polym. Sci.,* **21,** 381 (1956).
13. M. Matsui, *Trans. Soc. Rheol.,* **20,** 465 (1976).
14. A. Ziabicki and L. Jarecki, in *High-Speed Fiber Spinning,* A. Ziabicki and H. Kawai, Eds., Interscience, New York, 1985, Chap. 9.
15. R. J. Samuels, *J. Polym. Sci.,* **P-A2,** 781 (1972).
16. A. Peterlin, *J. Polym. Sci.,* **A-2,** 1511 (1969).
17. P. B. Rim and C. J. Nelson, *J. Appl. Polym. Sci.,* **42,** 1807 (1991).
18. R. S. Stein and F. H. Norris, *J. Polym. Sci.,* **21,** 381 (1956).
19. B. Wunderlich, *Thermal Analysis,* Academic Press, New York, 1990, Chap. 6.
20. T. Murayama, *Dynamic Mechanical Analysis of Polymeric Material,* Elsevier, New York, 1978.
21. S. Manabe and K. Kamide, *Polym. J.,* **16,** 375 (1984).
22. M. Takayanagi, *Viscoelastic Properties Crystal. Polym.,* **1,** 3 (1963).
23. M. Takayanagi and T. Matsuo, *J. Macromol. Sci., Phys.,* **B1,** 407 (1967).
24. Y. Fu, W. R. Busing, Y. Jin, K. A. Affholter, and B. Wunderlich, *Makromol. Chem.,* **195,** 803 (1994).
25. J. Shimizu, *Sen-i Kikai Gakkaishi,* **38,** 243 (1985).
26. J. P. Bell and J. H. Dumbleton, *J. Polym. Sci.,* **A-2,** 1033 (1969).
27. J. P. Bell and T. Murayama, *J. Polym. Sci.,* **A-2,** 1059 (1969).
28. G. E. Sweet and J. P. Bell, *J. Polym. Sci.,* **A-2,** 1273 (1972).
29. P. J. Holdsworth and A. Turner–Jones, *Polymer,* **12,** 195 (1971).
30. D. L. Nealy, T. G. Davis, and C. J. Kibler, *J. Polym. Sci.,* **A-2,** 2141 (1970).
31. K. M. Gupte, H. Motz, and J. M. Schultz, *J. Polym. Sci., Polym. Phys. Ed.,* **21,** 1927 (1983).
32. G. Perez, in *High-Speed Fiber Spinning,* A. Ziabicki and H. Kawai, Eds., Interscience, New York, 1985, Chap. 12.
33. J. Shimizu, N. Okui, and T. Kikutani, in *High-Speed Fiber Spinning,* A. Ziabicki and H. Kawai, Eds., Interscience, New York, 1985, Chap. 15.
34. H. Davis, *ARS Textrina,* **12,** 23 (1989).
35. Y. Fu, B. Annis, A. Boller, Y. Jin, and B. Wunderlich, *J. Polym. Sci., Polym. Phys. Ed.,* **32,** 2289 (1994).
36. T. Thistlethwaite, R. Jakeways, and I. M. Ward, *Polymer,* **29,** 61 (1988).
37. H. Chang, K. G. Lee, and J. M. Schultz, *J. Macromol. Sci., Phys.,* **B33,** 105 (1994).
38. K. L. Peng and C. M. Roland, *J. Polym. Sci., Polym. Phys. Ed.,* **31,** 1339 (1993).
39. D. W. Tomlin, C. M. Roland, and L. I. Slutsker, *J. Polym. Sci., Polym. Phys. Ed.,* **31,** 1331 (1993).
40. V. I. Gerasimov, Y. V. Genin, A. I. Kitaigorodsky, and D. Y. Tsvankin, *Kolloid-Z. Z. Polym.,* **250,** 518 (1972).